Atmos. Chem. Phys. Discuss., 9, 22865–22881, 2009
www.atmos-chem-phys-discuss.net/9/22865/2009/

Atmospheric Chemistry and Physics Discussions

This discussion paper is/has been under review for the journal *Atmospheric Chemistry and Physics (ACP)*. Please refer to the corresponding final paper in *ACP* if available.

Effects of resolution on the relative importance of numerical and physical diffusion in atmospheric composition modelling

M. D'Isidoro, A. Maurizi, and F. Tampieri

CNR-ISAC, via Gobetti 101, 40129 Bologna, Italy

Received: 11 September 2009 – Accepted: 13 October 2009 – Published: 28 October 2009

Correspondence to: M. D'Isidoro (m.disidoro@isac.cnr.it)

Published by Copernicus Publications on behalf of the European Geosciences Union.

Abstract

Numerical diffusion induced by advection has a large influence on concentration of substances in atmospheric composition models. At coarse resolutions numerical effects dominate, whereas at increasing model resolutions a description of physical diffusion is needed. The effects of changing resolution and Courant number are investigated for the WAF advection scheme (used in BOLCHEM), evidencing a sub-diffusive process. The spreading rate from an instantaneous source is compared with the physical diffusion necessary to simulate unresolved turbulent motions. The time at which the physical diffusion process overpowers the numerical spreading is estimated, and is shown to reduce as the resolution increases, and to increase with wind velocity.

1 Introduction

Sub-grid parameterization is a key issue in air quality modelling, as many physical processes occur at smaller scales than that resolved by the models. Equations solved in numerical simulations are smoothed in order to remove the finer structures from the solution. This inhability of models to resolve the smaller scales of motion implies the use of diffusion parameterizations. Broadly speaking, this smoothing is the same as to applying a filter in the wavenumber space, retaining only small wavenumbers. This procedure has recently been reviewed by Wyngaard (2004).

From the numerical point of view, the need to inhibit the growth of instabilities in the solution for the dynamical fields may be satisfied in ways other than parameterising the physical diffusion due to unresolved scales. The numerical issue is tackled using hyperdiffusion (e.g. Knievel et al., 2007; Bryan et al., 2003) terms and/or appropriate advection schemes. Passive tracers do not in principle need smoothing but it is also known that different advection schemes induce numerical diffusion effects per se, even if no explicit smoothing is prescribed. Odman (1997) analysed from a numerical point of view the implicit diffusion introduced by four different advection schemes. A systematic

ACPD

9, 22865–22881, 2009

analysis of the relative importance between numerical and physical diffusion at different spatial resolutions is in order.

The present work concentrates on horizontal diffusion and addresses the issue of the competition between physical diffusion (due to the parameterisation of sub-grid motions) and numerical diffusion (intrinsic in the numerical scheme or induced by hyperdiffusion terms) for a given advection scheme. In particular we consider the mass conservative Weighted Average Flux (WAF) advection scheme (Billet and Toro, 1997) adopted in the BOLCHEM model (Mircea et al., 2008), applying the algorithm to an idealised tracer distribution.

The paper is organized as follows. In Sect. 2 a parameterisation of diffusion arising from unresolved turbulent motions is discussed, as a paradigm of physical dispersion. In Sect. 3 the numerical aspects are dealt with. Subsequently, Sect. 4 presents some numerical simulations for an idealized case, in order to establish a general frame for the evaluation of the numerical vs. physical effects of the diffusion. Finally, some conclusions are drawn.

2 Sub-grid turbulent diffusion

In the present study the effect of unresolved (sub-grid) scales of turbulent motion on dispersion can be represented by a sub-grid turbulent diffusion coefficient D_H, where the subscript H emphasises the fact that only horizontal diffusion is considered. D_H can be estimated at a given resolution when the properties of turbulence at the scale of the resolution are known.

Assuming a Kolmogorov (1941) (K41) spectrum, D_H as a function of the wavenumber is given by

$$D_H(k) = \frac{9}{2}\frac{C_1^2}{C_0}\varepsilon^{1/3}k^{-4/3} \quad (1)$$

ACPD
9, 22865–22881, 2009

where $C_1=0.25\,C_K$ ($C_K=2$), $C_0=6.2$ is the Lagrangian structure function constant, and ε can be determined from velocity spectra measured in a variety of flow conditions and experimental arrangements. Following the Tampieri and Maurizi (2007) recipe, in the boundary layer ($z<h$) we have:

– unstable conditions Albertson et al. (1997):

$$\varepsilon=\frac{u_*^3}{\kappa\tilde{z}}\left(0.61-1.75\frac{\tilde{z}}{L_{\mathrm{MO}}}\right),\quad L_{\mathrm{MO}}<0 \tag{2}$$

– stable conditions (Pahlow et al., 2001):

$$\varepsilon=\frac{u_*^3}{\kappa\tilde{z}}\left(0.61-5\frac{\tilde{z}}{L_{\mathrm{MO}}}\right),\quad L_{\mathrm{MO}}>0 \tag{3}$$

where $\tilde{z}^{-1}=\ell_0^{-1}+z^{-1}$ in which $\ell_0=500\,\mathrm{m}$ is assumed; and L_{MO} is the Monin-Obukhov length.

while above the boundary layer ($z>h$) $\varepsilon=5.\times10^{-5}\mathrm{m}^2\mathrm{s}^{-3}$ is assumed as being representative of tropospheric data. For model applications, the height h can be determined case by case, using model profiles along with the actual stability.

As an example, in free-troposphere for a grid mesh size $\Delta x=10\,\mathrm{km}$, the Tampieri and Maurizi (2007) model gives $D_H=310\,\mathrm{m}^2\,\mathrm{s}^{-1}$.

3 Remarks on numerics

Let us consider the advection equation for the concentration $C(\mathbf{x},t)$ of a passive tracer:

$$\left(\frac{\partial}{\partial t}+\mathbf{U}\cdot\nabla\right)C=0 \tag{4}$$

where $\mathbf{U}$ is the prescribed velocity field.

ACPD
9, 22865–22881, 2009

The discretisation of Eq. (4) produces, in general, the spread of a cloud of tracer advected by the velocity field (see, e.g. Smolarkiewicz, 1984). The nature and magnitude of this spread is not only a function of the resolution, but also of the numerical scheme. For simplicity, the spread is referred to as numerical diffusion, regardless of the fact that the process may display or not diffusive behaviour, i.e. a growth of the cloud size σ proportional to the square root of time.

3.1 Non-dimensional form of advection equation

In order to identify the parameters relevant to the study of numerical diffusion, the source dimension R and the characteristic wind speed U are selected as scales for length and velocity, respectively, to give Eq. (4) the non dimensional form:

$$(\frac{\partial}{\partial t'} + \frac{UT}{R}\mathbf{U}'\cdot\nabla')C'=0 \tag{5}$$

where the prime indicates non-dimensional quantities and operators. The time scale must be defined as $T=RU^{-1}$ to make Eq. (5) scale-invariant.

In order to solve Eq. (5) numerically, space-time are discretised by Δx and Δt, respectively. Combining the non-dimensional grid mesh size $\Delta x'=R^{-1}\Delta x$ and time step $\Delta t'=UR^{-1}\Delta t$, we define the following set of non-dimensional parameters: the resolution

$$\rho=\frac{R}{\Delta x} \equiv (\Delta x')^{-1} \tag{6}$$

and the Courant number

$$v=\frac{\Delta t\, U}{\Delta x} \equiv (\Delta t')(\Delta x')^{-1}. \tag{7}$$

ACPD
9, 22865–22881, 2009

Using these parameters, the non-dimensional time is expressed by

$$t' = N v \rho^{-1} \tag{8}$$

where $N = t\Delta t^{-1}$ represents the number of integration steps.

Any solution of Eq. (5) depends on two parameters only, as does the increase in variance σ^2 of the tracer distribution $C(\mathbf{x}, t)$ with respect to its initial value, which in non-dimensional terms, reads

$$\Delta\sigma'^2(t'; \rho, v) = \frac{\sigma^2(t') - \sigma^2(t_0)}{R^2}. \tag{9}$$

3.2 Weighted Average Flux advection scheme

In the present study use is made of a mass conservative advection algorithm based on the WAF numerical scheme (Billet and Toro, 1997), which is briefly described below.

The advection Eq. (4) is solved numerically using an operator splitting approach, namely, by carrying out the computations for each of the space dimensions sequentially. Discretising in i-th direction in space one obtains

$$C_i^{n+1} = C_i^n - \frac{\Delta t}{\Delta x_i}(f^*_{i+1/2} - f^*_{i-1/2}) \tag{10}$$

where f^* is the numerical WAF flux (Hubbard and Nikiforakis, 2003) defined as

$$f^*_{i+1/2} = \frac{1}{2}(1 + \phi_{i+1/2})f_i + \frac{1}{2}(1 + \phi_{i-1/2})f_{i+1} \tag{11}$$

and ϕ_i are "limiter functions", which have in general the form of an amplification factor applied to the Courant number v. In order to eliminate undesired oscillations from the solution, the limiter functions are defined to be function also of the local flow parameter $r = \Delta C_{\text{upwind}}/\Delta C_{\text{local}}$, which avoids spurious oscillations by adding a numerical dissipation. The limiter functions are defined as

$$\phi(r, v) = \text{sgn}(v)[1 + (|v| - 1)b] \tag{12}$$

ACPD
9, 22865–22881, 2009

where

$$b = \max[0, \min(2r, 1), \min(r, 2)]. \quad (13)$$

Given the above hypotheses, the resulting WAF advection scheme is second order accurate in space (first in time) and mass conservative.

4 Results and discussion

In order to evaluate the effect of numerical diffusion, several numerical tests were performed for different grid resolutions and Courant numbers. A simplified framework was chosen, with wind field $(u, v)=(U, 0)$, in order to single out the effects of sub-grid processes. The initial tracer distribution was chosen with Gaussian-shape and standard deviation $\sigma_0=R$. Aiming to measure the effect of numerical diffusion as a function of the mass distribution resolution, the numerical tests were set up varying the two parameters ρ and v. Experiments are summarised in Table 1.

Figure 1 shows the increase of normalised puff variance with non-dimensional time for different values of ρ (a) and v (b). Variations of ρ induce large variations of $\Delta\sigma'^2$, while varying v has a weaker impact. In the following v is fixed to 0.6 to simplify the analysis.

For large non-dimensional time, say $\mathcal{O}(100)$, it can be assumed that the increase of variance with time can be well approximated by a power law:

$$\Delta\sigma'^2 = \alpha t'^{\beta}. \quad (14)$$

Fitting Eq. (14) on data allows the determination of both slope β and "diffusion coefficient" α. The results are reported in Fig. 2a and b for different ρ.

Although β varies, its variation is sufficiently small to justify the direct comparison of α in Fig. 2a.

It is worth noting that the representative value of β highlights the sub-diffusive nature of the numerical diffusion process. The magnitude of this process is largely driven by

ACPD
9, 22865–22881, 2009

resolution, as shown in Fig. 2a, where the sub-diffusion coefficient α varies by orders of magnitude with ρ. This suggests that conditions can be met for physical diffusion ($\propto t'$) to become dominant, depending on the numerical resolution.

In order to give an idea of what those conditions are, a direct comparison with the sub-grid turbulent diffusion described in Sect. 2 was performed.

The increase of non-dimensional variance for the turbulent (Lagrangian) diffusion process is expressed by

$$\Delta\sigma'^2_L = \frac{2Dt}{R^2} = 2D't' \tag{15}$$

where $D'=D(RU)^{-1}$ is the non-dimensional sub-grid diffusion coefficient, which is a function of Δx. Assuming that the wavenumber is $k=\pi(\Delta x)^{-1}$, from Eq. (1) D' can be expressed by

$$D = \gamma \frac{(\varepsilon R)}{U}^{1/3} \rho^{-4/3} \tag{16}$$

where $\gamma=(9/2)\pi^{-4/3}(0.25\,C_K)^2 C_0^{-1}$. Note that since the turbulent dispersion process does not depend on U and R, the non-dimensionalisation makes D' explicitly dependent on them. Therefore, in order to compare the results of the numerical and turbulent processes, R and U must be selected. Here R, representing the source scale, is given a fixed value, $\tilde{R}=12\,500$ m, which is representative of the resolution for regional air quality models, for which the sub-grid sources are distributed instantaneously over the grid, limiting this way the size of the source itself. U is left to vary in a typical range from 1 to 20 ms^{-1}.

Figure 3a–d show $\Delta\sigma'^2_L(\tilde{R},U)$ for different resolutions (ρ=2, 1.5, 1, and 0.5, respectively), each for different values of U, along with $\Delta\sigma'^2$ for comparison.

The intersection between $\Delta\sigma'^2$ and $\Delta\sigma'^2_L(\tilde{R},U)$ defines the time at which turbulent diffusion starts to dominate over numerical sub-diffusion. Increasing resolution reduces both variances but, due to the different dependence on ρ, the numerical sub-diffusion

ACPD
9, 22865–22881, 2009

coefficient declines more rapidly than the turbulent diffusion coefficient. This makes high-resolution simulations more sensitive to turbulence parameterisation. Furthermore, for low wind velocity it occurs in a shorter time. In fact, in the limit $U \rightarrow 0$, the numerical effects on diffusion vanish.

The non-dimensional time τ at which the size of the puff is equal for the numerical and turbulent diffusion processes can be computed combining Eqs. (14) and (15) by

$$\tau = \left(\frac{2D'(\rho, \tilde{R}, U)}{\alpha(\rho)} \right)^{(\beta(\rho)-1)^{-1}} \quad (17)$$

Figure 4a and b report τ, as a function of ρ (for given $\tilde{R}$) for fixed ν=0.6 (varying U) and fixed U=5 ms^{-1} (varying ν), respectively. It is worth noting that wind velocity variations play a major role in determining τ with respect to ν variations, especially for resolutions below $\mathcal{O}(1)$. For higher resolutions however, τ decreases rapidly.

A factor to be taken into account is that for a given grid mesh size Δx, even in the case where an explicit description of the unresolved energy through a sub-grid scale model is given, the range in which energy spectrum is not well represented extends up to 6 Δx (Bryan et al., 2003). The energy accounted for the explicit solution of primitive equations is therefore less than that expected from a K41 in the high-wavenumber end of the spectrum. This means that the diffusion coefficient D estimated from Eq. (1), which implies a "perfect" sub-grid model, is probably underestimated, making the results biased towards an underestimation of physical diffusion and then an overestimation of τ. With the present value of the source size R and for grid mesh size between 5 and 20 km (typical of hydrostatic models) the numerical diffusion overpowers the physical one for values of τ approximately between 1 and 10^4, corresponding to few hours to days. Thus the gradients are excessively smoothed and there is no room for a more physical description of the dispersion process.

Preliminary experiments conducted for ρ=3 show that τ drops of order of magnitude. Thus for finer grid mesh sizes (~1 km) the role of physical diffusion becomes more and

ACPD
9, 22865–22881, 2009

more important. This requires the extension of the present study to values of resolution ρ above 3, going in the range attainable by non-hydrostatic models.

Another remark is in order regarding current air quality simulations: the resolution ρ is always about 1 because scales of sources are much smaller than the grid mesh size. This means that in this kind of simulations, numerical diffusion is always dominating over the physical one, even for very low wind velocity.

5 Conclusions

The present article has considered the horizontal spread of a tracer released instantaneously in a uniform wind field, to study the diffusion induced by the numerical advection scheme WAF in comparison with the sub-grid physical diffusion. It has been found that:

- numerical diffusion depends on only two parameters: resolution and Courant number;
- numerical spread induced by WAF is sub-diffusive;
- resolution plays a major role, respect to variations induced by the Courant number (see Fig. 1);
- the time at which physical diffusion starts to be larger than numerical diffusion decreases as the resolution increases (see Fig. 4);
- the said time is further reduced in low wind conditions and large Courant number.

Due to the dominance of numerical diffusion over physical one for typical air quality model resolutions, further investigations on less diffusive advection schemes is mandatory.

Acknowledgements. The authors would like to thank Piero Malguzzi for his valuable support. This work was supported by the FP6 IP GEMS and FP7 CITYZEN. Partial support from the Italia-USA Cooperation Agreement on Science and Technology of Climate Change is also acknowledged.

References

Albertson, J. D., Parlange, M. B., Kiely, G., and Eichinger, W. E.: The average dissipation rate of turbulent kinetic energy in the neutral and unstable atmospheric surface layer, J. Geophys. Res., 102, 13423–13432, 1997. 22868

Billet, S. J. and Toro, E. F.: On WAF-Type Schemes for Multidimensional Hyperbolic Conservation Laws, J. Comput. Phys., 130, 1–24, 1997. 22867, 22870

Bryan, G. H., Wyngaard, J. C., and Fritsch, J. M.: Resolution Requirements for the Simulation of Deep Moist Convection, Mon. Weather Rev., 131, 2394–2416, 2003. 22866, 22873

Hubbard, M. E. and Nikiforakis, N.: A Three-Dimensional, Adaptive, Godunov-Type Model for Global Atmospheric Flows, Mon. Weather Rev., 131, 1848–1864, 2003. 22870

Knievel, J. C., Bryan, G. H., and Hacker, J. P.: Explicit Numerical Diffusion in the WRF Model, Mon. Weather Rev., 135, 3808–3824, doi:10.1175/2007mwr2100.1, 2007. 22866

Kolmogorov, A. N.: The local structure of turbulence in incompressible viscous fluid for very large Reynolds numbers, Dokl. Akad. Nauk. SSSR, 30, 301, 1941. 22867

Mircea, M., D'Isidoro, M., Maurizi, A., Vitali, L., Monforti, F., Zanini, G., and Tampieri, F.: A comprehensive performance evaluation of the air quality model BOLCHEM to reproduce the ozone concentrations over Italy, Atmos. Environ., 42, 1169–1185, 2008. 22867

Odman, M. T.: A Quantitative Analysis Of Numerical Diffusion Introduced By Advection Algorithms In Air Quality Models, Atmos. Environ., 31, 1933–1940, 1997. 22866

Pahlow, M., Parlange, M. B., and Porte-Agel, F.: On Monin-Obukhov similarity in the stable atmospheric boundary layer, Bound.-Lay. Meteorol., 99, 225–248, 2001. 22868

Smolarkiewicz, P. K.: A Fully Multidimensional Positive Definite Advection Transport Algorithm with Small Implicit Diffusion, J. Comp. Phys., 54, 325–362, 1984. 22869

Tampieri, F. and Maurizi, A.: Evaluation of the dispersion coefficient for numerical simulations of tropospheric transport, Nuovo Cimento C, 30, 395–406, 2007. 22868
Wyngaard, J. C.: Toward numerical modelling in the “terra incognita”, J. Atmos. Sci., 61, 1816–1826, 2004. 22866

Table 1. Summary of the numerical experiments performed, showing parameters ρ and v. Experiments are organised in groups (A to I), each characterised by a given ρ. The suffix numbers used in the text indicate the values of ρ and v, respectively, used for each experiment.

Exp.	Resol. (ρ)	Courant (v)					
$A_{\rho,v}$	2.5	0.1,	0.2,	0.4,	0.6,	0.8,	0.9
$B_{\rho,v}$	2	0.1,	0.2,	0.4,	0.6,	0.8,	0.9
$C_{\rho,v}$	1.5	0.1,	0.2,	0.4,	0.6,	0.8,	0.9
$D_{\rho,v}$	1	0.1,	0.2,	0.4,	0.6,	0.8,	0.9
$E_{\rho,v}$	0.7	0.1,	0.2,	0.4,	0.6,	0.8,	0.9
$F_{\rho,v}$	0.5	0.1,	0.2,	0.4,	0.6,	0.8,	0.9
$G_{\rho,v}$	0.4	0.1,	0.2,	0.4,	0.6,	0.8,	0.9
$H_{\rho,v}$	0.25	0.1,	0.2,	0.4,	0.6,	0.8,	0.9
$I_{\rho,v}$	0.125	0.1,	0.2,	0.4,	0.6,	0.8,	0.9

ACPD
9, 22865–22881, 2009

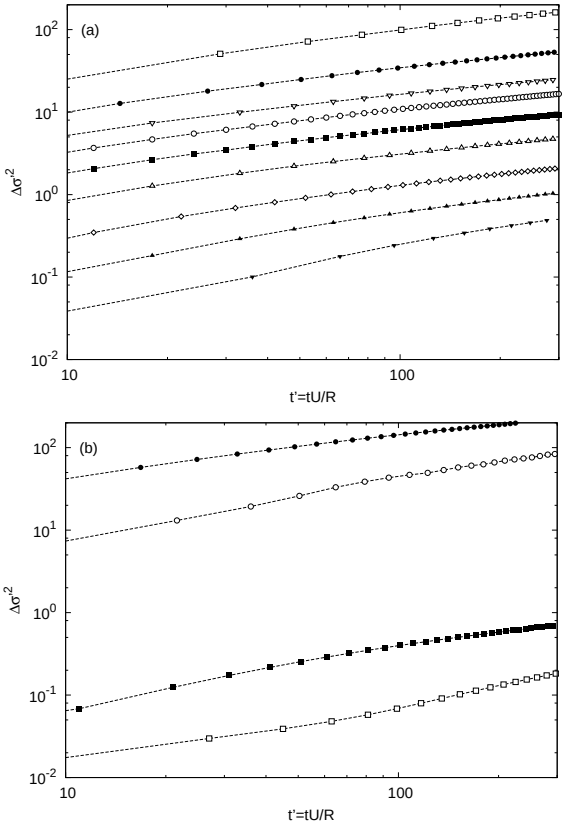

Fig. 1. **(a)** Normalised variance as a function of non-dimensional time t' for different values of ρ: starting from bottom to top the curves refer to experiments $A_{\rho 2.5,\nu 0.6}$, $B_{\rho 2,\nu 0.6}$, $C_{\rho 1.5,\nu 0.6}$, $D_{\rho 1,\nu 0.6}$, $E_{\rho 0.7,\nu 0.6}$, $F_{\rho 0.5,\nu 0.6}$, $G_{\rho 0.4,\nu 0.6}$, $H_{\rho 0.25,\nu 0.6}$ and $I_{\rho 0.125,\nu 0.6}$, respectively. **(b)** The same as (a) but for experiments with the same ρ and different values of ν: $I_{\rho 0.125,\nu 0.1}$ and $I_{\rho 0.125,\nu 0.9}$, black and white circles, respectively; $A_{\rho 2.5,\nu 0.1}$ and $A_{\rho 2.5,\nu 0.9}$, black and white squares, respectively.

ACPD
9, 22865–22881, 2009

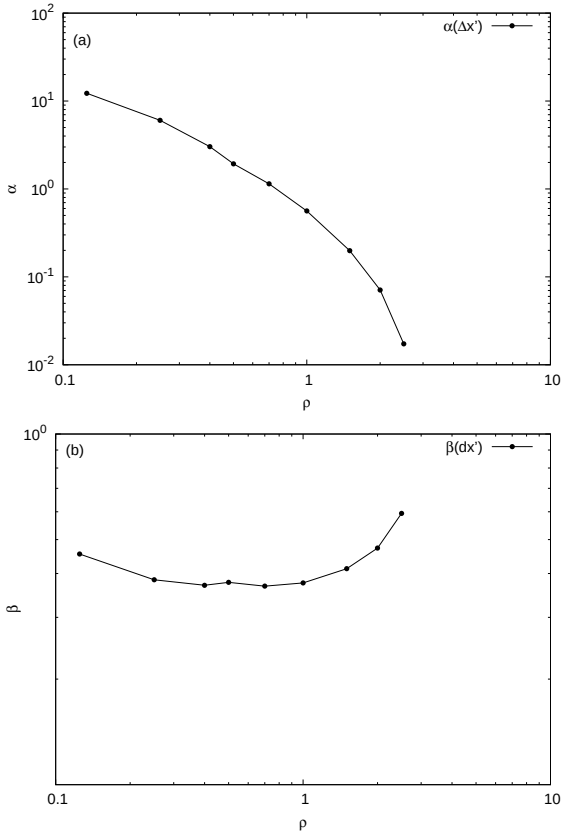

Fig. 2. Coefficient α **(a)** and exponent β **(b)** of Eq. (14), as a function of ρ.

ACPD
9, 22865–22881, 2009

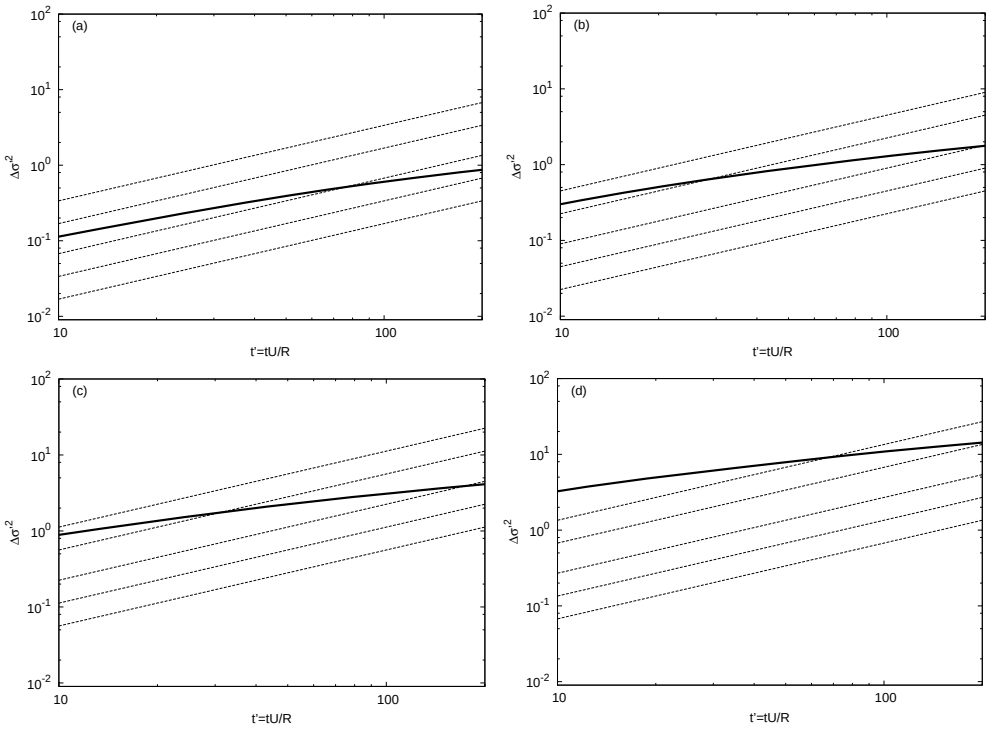

Fig. 3. Comparison of numerical (continuous line) and physical diffusion (dashed lines) for different wind velocities, for four resolutions: **(a)** $B_{\rho 2,v0.6}$; **(b)** $C_{\rho 1.5,v0.6}$; **(c)** $D_{\rho 1,v0.6}$ and **(d)** $F_{\rho 0.5,v0.6}$. Dashed lines represent, from top to bottom, physical diffusion for U=1, 2, 5, 10, 20 ms^{-1}.

ACPD
9, 22865–22881, 2009

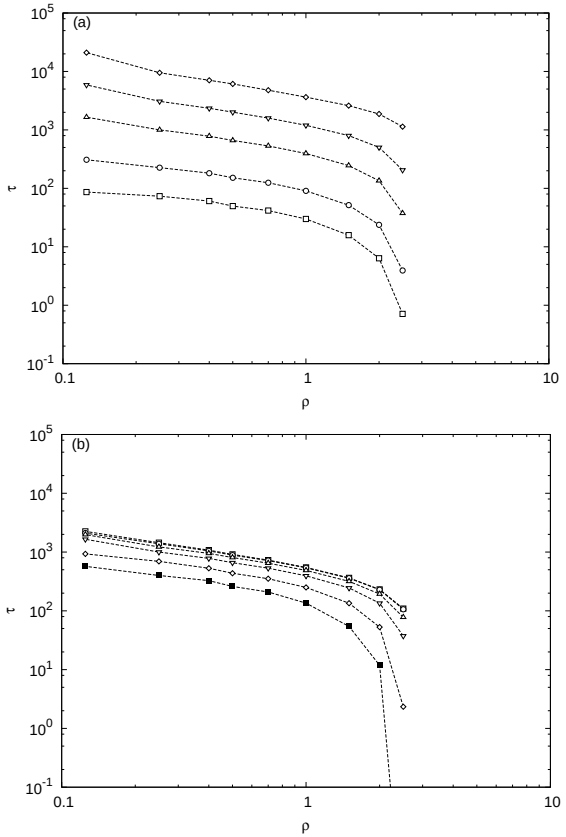

Fig. 4. Non-dimensional time τ, as a function of ρ, computed (for given $\tilde{R}$) for different conditions: curves in **(a)** refers to fixed v=0.6 and varying U=20, 10, 5, 2, 1 ms^{-1} from top to bottom, respectively. Curves in **(b)** refers to fixed U=5 ms^{-1} and varying v=0.1, 0.2, 0.4, 0.6, 0.8, 0.9 from top to bottom, respectively.

ACPD
9, 22865–22881, 2009